AGU ADVANCING EARTH AND SPACE SCIENCES

Geophysical Research Letters®

RESEARCH LETTER
10.1029/2023GL104848

Historical Changes and Reasons for Model Differences in Anthropogenic Aerosol Forcing in CMIP6

Stephanie Fiedler[1,2], Twan van Noije[3], Christopher J. Smith[4,5], Olivier Boucher[6], Jean-Louis Dufresne[7], Alf Kirkevåg[8], Dirk Olivié[8], Rovina Pinto[9], Thomas Reerink[3], Adriana Sima[7], and Michael Schulz[8]

[1]GEOMAR Helmholtz Centre for Ocean Research Kiel, Kiel, Germany, [2]Faculty of Mathematics and Natural Sciences, Christian-Albrechts-University of Kiel, Kiel, Germany, [3]Royal Netherlands Meteorological Institute, De Bilt, The Netherlands, [4]Priestley International Centre for Climate, University of Leeds, Leeds, UK, [5]Energy, Climate and Environment Program, International Institute for Applied Systems Analysis, Laxenburg, Austria, [6]Institut Pierre-Simon Laplace, Sorbonne Université / CNRS, Paris, France, [7]Laboratoire de Météorologie Dynamique (LMD)/Institut Pierre Simon Laplace (IPSL), Sorbonne Université/CNRS/École Normale Supérieure/École Polytechnique, Paris, France, [8]Norwegian Meteorological Institute, Oslo, Norway, [9]University of Cologne, Institute of Geophysics and Meteorology, Cologne, Germany

Abstract The Radiative Forcing Model Intercomparison Project (RFMIP) allows estimates of effective radiative forcing (ERF) in the Coupled Model Intercomparison Project phase six (CMIP6). We analyze the RFMIP output, including the new experiments from models that use the same parameterization for anthropogenic aerosols (RFMIP-SpAer), to characterize and better understand model differences in aerosol ERF. We find little changes in the aerosol ERF for 1970–2014 in the CMIP6 multi-model mean, which implies greenhouse gases primarily explain the positive trend in the total anthropogenic ERF. Cloud-mediated effects dominate the present-day aerosol ERF in most models. The results highlight a regional increase in marine cloudiness due to aerosols, despite suppressed cloud lifetime effects in that RFMIP-SpAer experiment. Negative cloud-mediated effects mask positive direct effects in many models, which arise from strong anthropogenic aerosol absorption. The findings suggest opportunities to better constrain simulated ERF by revisiting the optical properties and long-range transport of aerosols.

Plain Language Summary Aerosols are particles in the atmosphere with sizes ranging from nanometers to tens of micrometers, which are emitted by natural and anthropogenic processes or formed from gases in the atmosphere. The extent to which anthropogenic aerosols affect the radiation budget of Earth is important to better understand anthropogenic climate changes. Aerosol effects on the radiation budget are simulated by complex Earth system models that informed the Sixth Assessment Report of the Intergovernmental Panel on Climate Change. Our study addresses why such model experiments show different magnitudes for aerosol radiative effects. The results point to opportunities to further improve models with existing observations of aerosol optical properties and aerosol transport over oceans in addition to the much-studied aerosol effects on clouds.

Key Points:

- Coupled Model Intercomparison Project phase six (CMIP6) averaged trend in aerosol effective radiative forcing (ERF) is small for 1970–2014 and weakly positive for 2000–2014
- Positive direct aerosol radiative effects in CMIP6 models are associated with strong aerosol absorption
- Diverse and often strong cloud-mediated effects primarily determine the magnitude of aerosol ERF in CMIP6

Supporting Information:

Supporting Information may be found in the online version of this article.

Correspondence to:

S. Fiedler,
sfiedler@geomar.de

Citation:

Fiedler, S., van Noije, T., Smith, C. J., Boucher, O., Dufresne, J.-L., Kirkevåg, A., et al. (2023). Historical changes and reasons for model differences in anthropogenic aerosol forcing in CMIP6. *Geophysical Research Letters*, *50*, e2023GL104848. https://doi.org/10.1029/2023GL104848

Received 7 MAR 2023
Accepted 14 JUL 2023

1. Introduction

Global climate models participating in the Coupled Model Intercomparison Project (CMIP) show differences in the radiative forcing of anthropogenic aerosols, which limits our ability to constrain the total anthropogenic radiative forcing (e.g., Bellouin et al., 2020; Myhre et al., 2013; Smith et al., 2020). Despite the implication for understanding and projecting climate changes, constraining the anthropogenic aerosol effective radiative forcing (aerosol ERF) using these models alone has been proven difficult. Model differences for aerosol ERF are a reflection of multiple difficulties in simulating aerosol effects concerning both the aerosols themselves and the meteorological processes interacting with them (e.g., Bony et al., 2015; Mülmenstädt et al., 2020; Neubauer et al., 2019; Samset et al., 2018; Stevens & Feingold, 2009; Voigt et al., 2021). Multiple plausible reasons for model differences in ERF exist, for example, the representation of aerosols, clouds, surface albedo, and radiation transfer (e.g., Boucher et al., 1998; Randles et al., 2013; Stier et al., 2013; Zanis et al., 2020). However, the understanding of how such model differences influence the simulated aerosol ERF is incomplete. A systematic assessment of the relative importance of involved processes contributing to model differences in aerosol ERF would help to develop a strategy for prioritizing efforts for improved climate experiments.

The Radiative Forcing Model Intercomparison Project (RFMIP, Pincus et al., 2016), endorsed by CMIP phase six (CMIP6, Eyring et al., 2016), provides a basis for a first systematic assessment of model differences in ERF from CMIP-class models. Through atmosphere-only experiments, RFMIP facilitated the quantification of ERF in CMIP6 models (RFMIP-ERF, Smith et al., 2020). All RFMIP-ERF experiments are carried out with global models in their standard configurations for CMIP6. Another part of RFMIP requested experiments with prescribed aerosol optical properties and aerosol effects on clouds by implementing the same parameterization (Stevens et al., 2017) in the participating models (RFMIP-SpAer). We assess the present-day aerosol ERF in RFMIP-SpAer experiments for the first time and put the results into the perspective of results from RFMIP-ERF, based on now more model experiments. Our approach allows us to discuss contributions to model differences in aerosol ERF and explore to what extent the insights can guide future model improvements.

2. Methods

We calculate ERF as the change in the net radiation flux at the top of the atmosphere (TOA) to an imposed spatiotemporally dependent anthropogenic perturbation in the atmospheric composition using model experiments. The design of these experiments complies with the RFMIP protocol (Pincus et al., 2016), that is, all models performed atmosphere-only experiments with prescribed sea-surface temperatures and sea ice. The experiments are performed for several decades to reduce the impact of model-internal variability on the ERF estimates (e.g., Fiedler et al., 2017; Forster et al., 2016). The CMIP6 models EC-Earth3 (Döscher et al., 2022), IPSL-CM6A-LR (Boucher et al., 2020), MPI-ESM1.2-LR (Mauritsen et al., 2019), and two configurations of NorESM2-LM (Seland et al., 2020) performed experiments for RFMIP-SpAer. The same parameterization for anthropogenic aerosols (MACv2-SP, Stevens et al., 2017) was implemented in the models for RFMIP-SpAer experiments. For IPSL-CM6A-LR and NorESM2-LM, it implies that the native anthropogenic aerosol parameterizations were switched off for emissions after 1850. In EC-Earth3 and MPI-ESM1.2-LR, MACv2-SP is part of the standard configuration for CMIP6.

The aerosol effect on clouds is parameterized by multiplying the cloud droplet number concentration (N) of the host model with the factor η_N from MACv2-SP, assessed in Fiedler et al. (2017). In all RFMIP-SpAer models except EC-Earth3, η_N is used to induce a Twomey effect (Twomey, 1974). It is accomplished by multiplying η_N with N directly in the radiation transfer calculation. EC-Earth3 additionally accounts for adjustments from aerosol-cloud interactions (*aci*) through the multiplication of η_N with N in the cloud microphysics (Döscher et al., 2022).

Differences in aerosol ERF arising from parameterizations of anthropogenic aerosols are evaluated by comparing results between RFMIP-SpAer and RFMIP-ERF. The assessment is systematic to the extent that we compare similar models from RFMIP-SpAer and RFMIP-ERF. Our intercomparison includes a separation of effective radiative effects into instantaneous radiative effects and net contributions from adjustments, as well as net contributions from clear and cloudy skies to infer where and why model differences arise. We further apply the method by Ghan (2013) to isolate cloud-mediated effects and analyze aerosol optical properties from all experiments for which the necessary diagnostic output is available. The methods are described in more detail in Supporting Information S1.

3. Results

3.1. Decadal Changes in ERF

The increasingly negative aerosol ERF in all-sky conditions at TOA in the CMIP6 multi-model mean can explain the stabilization of the total anthropogenic ERF between the 1930s and the 1960s (Figures 1a and 1b). The aerosol ERF trend averaged for RFMIP-ERF is -0.013 ± 0.005 Wm^{-2} yr^{-1} (multi-model mean $\pm$ inter-model standard deviation) for 1930–1960 (Table S1 in Supporting Information S1). In the same period, the trend in the total anthropogenic ERF is 0.004 ± 0.003 Wm^{-2} yr^{-1} which is an order of magnitude smaller, suggesting that aerosol ERF to a large degree offset the expected ERF increase associated with increasing greenhouse gas (GHG) forcing. Having a near-constant total anthropogenic ERF in the CMIP6 multi-model mean implies slower warming during that time period, consistent with temperature observations (Gulev et al., 2021).

The change in the aerosol ERF in the CMIP6 multi-model mean over the past five decades is small compared to the inter-model range (maximum minus minimum) in aerosol ERF. Specifically, there is little change in the

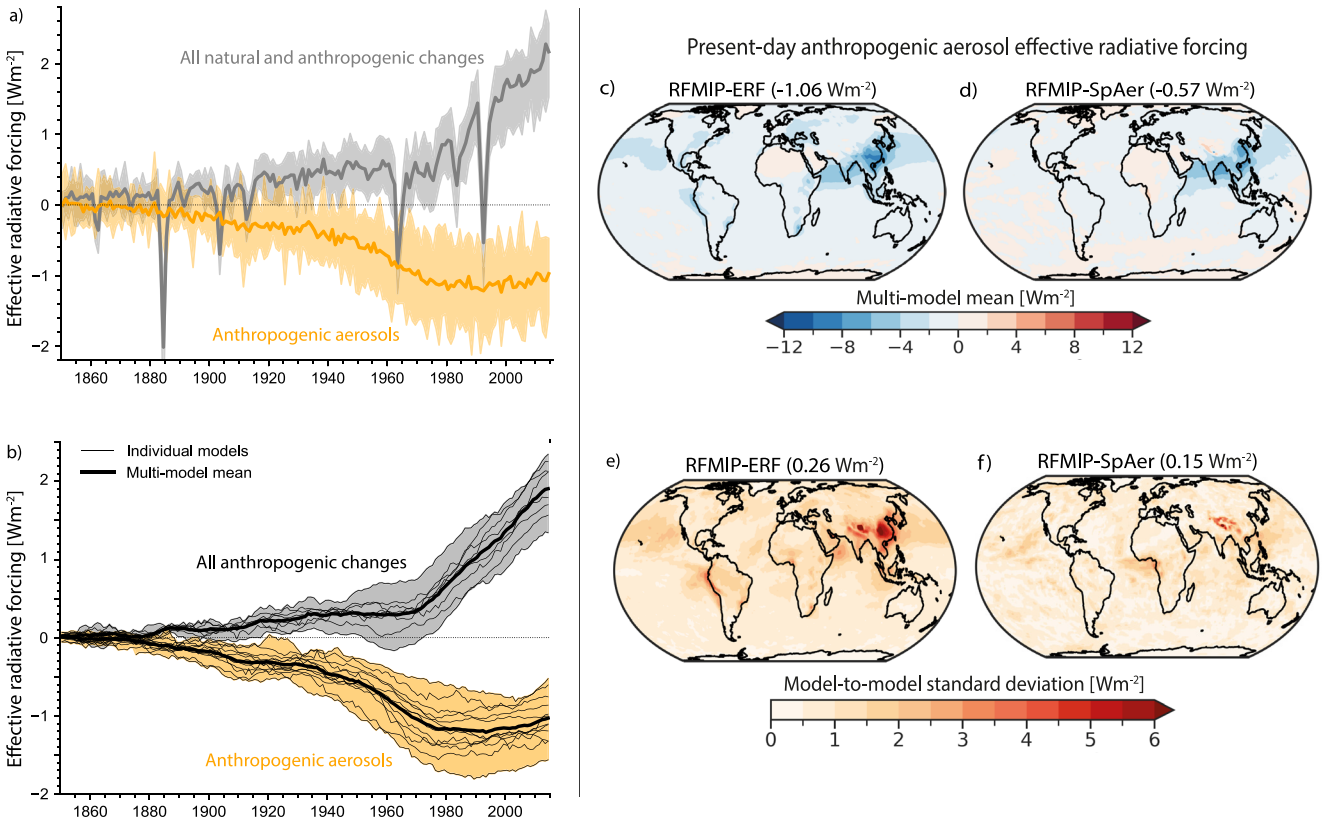

Figure 1. Effective radiative forcing from CMIP6 models. Shown are the (a) global annual means of ERF for (gray) all-natural plus anthropogenic changes taken together and (orange) anthropogenic aerosols only, (b) global eleven-year running means of ERF for (gray) all anthropogenic changes and (orange) anthropogenic aerosols only, (c–d) multi-model mean of regional contributions to the aerosol ERF for 2014, and (e–f) inter-model standard deviations in regional contributions to aerosol ERF for 2014. All values are for all sky at the top of the atmosphere (TOA) from CMIP6 models that performed experiments for RFMIP. Available model experiments for a–b and c–f are listed in Tables S1 and S2, respectively, in Supporting Information S1. Shading in a–b marks the model range and the thick lines are the multi-model means. The thin lines in b are results from individual models. Values in brackets in (c–f) are the global means.

eleven-year running means of aerosol ERF since the 1970s averaged across RFMIP-ERF (Figures 1a and 1b). The inter-model differences in aerosol ERF are comparably larger with an inter-model standard deviation of 0.26 Wm^{-2} in the present-day aerosol ERF, which corresponds to one quarter of the mean present-day aerosol ERF of -1.06 Wm^{-2}. The magnitude of present-day aerosol ERF in CMIP6 is also noticeably smaller compared to natural forcing from the three largest explosive volcanic eruptions, marked by sharp decreases in the total ERF (Figure 1a). The only slight change in the aerosol ERF in the past five decades in the CMIP6 multi-model mean occurs despite strong regional aerosol trends, documented elsewhere (e.g., Cherian & Quaas, 2020). Even the large differences in the global distribution of anthropogenic aerosol emissions as seen between the 1970s and 2000s have therefore no substantial influence on the aerosol ERF and hence total anthropogenic ERF in the CMIP6 multi-model mean, previously indicated by fewer models using MACv2-SP (Fiedler et al., 2017, 2019). The relatively stable aerosol ERF over the past 50 years in the CMIP6 multi-model mean implies that the sharp increase in total anthropogenic ERF by about 1.4 Wm^{-2} in the multi-model mean, namely from around 0.4 Wm^{-2} in the 1970s to 1.8 Wm^{-2} in 2014 (Figure 1b) is primarily driven by the increase in GHG concentrations in the atmosphere, despite regional changes in aerosol radiative effects (e.g., Fiedler et al., 2019).

A slightly positive trend in aerosol ERF occurs for 2000–2014 in the RFMIP-ERF mean, that is, aerosol ERF became less negative. In the CMIP6 multi-model mean, the negative trend in aerosol ERF stopped around the 1980s followed by the later slightly positive trend (Figure 1b), which is also seen in an energy-budget model (Smith et al., 2021). For 2000–2014, the RFMIP-ERF averaged trend in aerosol ERF is 0.007 ± 0.008 Wm^{-2} yr^{-1} (Table S1 in Supporting Information S1), consistent with observations (Quaas et al., 2022). Not all models have a positive 2000–2014 trend in aerosol ERF (NorESM2-LM, MIROC6, MPI-ESM1.2-LR). Some models with strongly negative trends in aerosol ERF for 1930–1960 have strongly positive trends for 2000–2014 (e.g.,

UKESM1-0-LL) but this is not always the case (e.g., MRI-ESM2-0, NorESM2-LM). Such differences can for instance arise from changes in simulated aerosol absorption. However, all models have a positive 2000–2014 trend in the total anthropogenic ERF with a multi-model mean of 0.035 ± 0.008 Wm^{-2} yr^{-1}, reflecting the dominant GHG forcing (Table S1 in Supporting Information S1).

Interestingly, some models simulate negative trends in the total anthropogenic ERF for 1930–1960 with near-zero or negative values in some years, which is in conflict with the common conclusion that the total anthropogenic ERF was positive throughout the 20th century. Take for instance the negative and close to zero total anthropogenic ERF around the 1960s in two CMIP6 models (Figure 1b), and negative trends in the total anthropogenic ERF for 1930–1960 (CNRM-CM6-1 and HadGEM3-GC31-LL, Table S1 in Supporting Information S1). The same models have a present-day aerosol ERF more negative than -1 Wm^{-2} (Table S2 in Supporting Information S1). Other models with a particularly strong negative trend in aerosol ERF for 1930–1960 (UKESM1-0-LL, NorESM2-LM, MRI-ESM2-0, and GISS-E2-1-G) also have a present-day aerosol ERF more negative than -1 Wm^{-2} (Tables S1 and S2 in Supporting Information S1). In the next section, we assess the model differences in the present-day aerosol ERF in more detail.

3.2. Present-Day Aerosol Radiative Effects

We diagnose an inter-model range in the aerosol ERF for present-day (2014) of -1.47 to -0.59 Wm^{-2} for RFMIP-ERF (Table S2 in Supporting Information S1). Most (15 out of 21) RFMIP-ERF models have an aerosol ERF more negative than -1 Wm^{-2}, also reflected in the RFMIP-ERF mean of -1.06 Wm^{-2}. Our model range in aerosol ERF is slightly larger compared to -1.37 to -0.63 Wm^{-2} from Smith et al. (2020), who had experiments from sixteen CMIP6 models plus one model with another configuration. With a total of now twenty models plus one additional model configuration, we confirm the smaller range in aerosol ERF in CMIP6, compared to CMIP5 estimates (Zelinka et al., 2014).

The present-day aerosol ERF is less negative and less diverse in RFMIP-SpAer compared to RFMIP-ERF. The model range in present-day aerosol ERF from RFMIP-SpAer of -0.79 to -0.46 Wm^{-2} (Table S2 in Supporting Information S1) falls onto the upper end of the range from RFMIP-ERF and within the range proposed by Stevens (2015). Changing the NorESM2-LM configuration from p1 to p2 has a marginal influence on ERF with a difference of 0.02 Wm^{-2} for the unified aerosols in RFMIP-SpAer (Table S2 in Supporting Information S1), but the two configurations lead to a ten-fold larger difference (0.2 Wm^{-2}) in aerosol ERF in RFMIP-ERF. The inter-model standard deviation is smaller in RFMIP-SpAer (0.15 Wm^{-2}) than in RFMIP-ERF (0.26 Wm^{-2}). The smaller aerosol ERF in RFMIP-SpAer experiments might be explained by the consistent implementation of aerosol effects in the models, with the largest differences arising from the aerosol effects on clouds. In most (3 of 4) RFMIP-SpAer models, the aerosol effect on clouds is induced in the radiation transfer calculation for a fixed liquid water content following ideas of Twomey (1974), and hence adjustments due to *aci* are suppressed. The only model in RFMIP-SpAer that simulates adjustment due to *aci* from MACv2-SP is EC-Earth3, which has the most negative aerosol ERF of -0.79 Wm^{-2} across the experiments in RFMIP-SpAer, but it is still less negative than the aerosol ERF in most (16 of 21) RFMIP-ERF models. The often more negative ERF in RFMIP-ERF could therefore be driven by stronger adjustments due to *aci* compared to RFMIP-SpAer, although this is not necessarily true for all models. All present-day aerosol ERF estimates from RFMIP-ERF and RFMIP-SpAer fall within the global bounds deduced from multiple lines of evidence by Bellouin et al. (2020). The plausibility should not be based on the global mean alone, because the spatial distribution of aerosols is important for regional climate responses (e.g., Deser et al., 2020; Kang et al., 2021; Liu et al., 2018; Wang & Wen, 2022; Wilcox et al., 2020).

The inter-model differences in the spatial distributions of the anthropogenic aerosol effective radiative effects for the present day are smaller when the anthropogenic aerosol representation is unified. We refer to these regional contributions to the aerosol ERF as aerosol $\mathcal{F}$. Some aspects of the spatial patterns in aerosol $\mathcal{F}$ are similar across RFMIP (Figure 1c–d), for example, regions with more negative aerosol $\mathcal{F}$ typically coincide with larger anthropogenic aerosol optical depth. The regional magnitudes of aerosol $\mathcal{F}$, however, substantially differ across RFMIP-ERF (Figure 1e). In RFMIP-SpAer, regional inter-model differences in aerosol $\mathcal{F}$ are comparably smaller (Figure 1f). Interestingly, the spatial extent of areas with negative aerosol $\mathcal{F}$ markedly reduces over oceans in the RFMIP-SpAer mean compared to the RFMIP-ERF mean, for example, over the Eastern North Pacific and the tropical North Atlantic (Figures 1c and 1d). Simulated patterns of aerosol $\mathcal{F}$, therefore, depend on the representation of aerosol effects over oceans downwind of continental pollution.

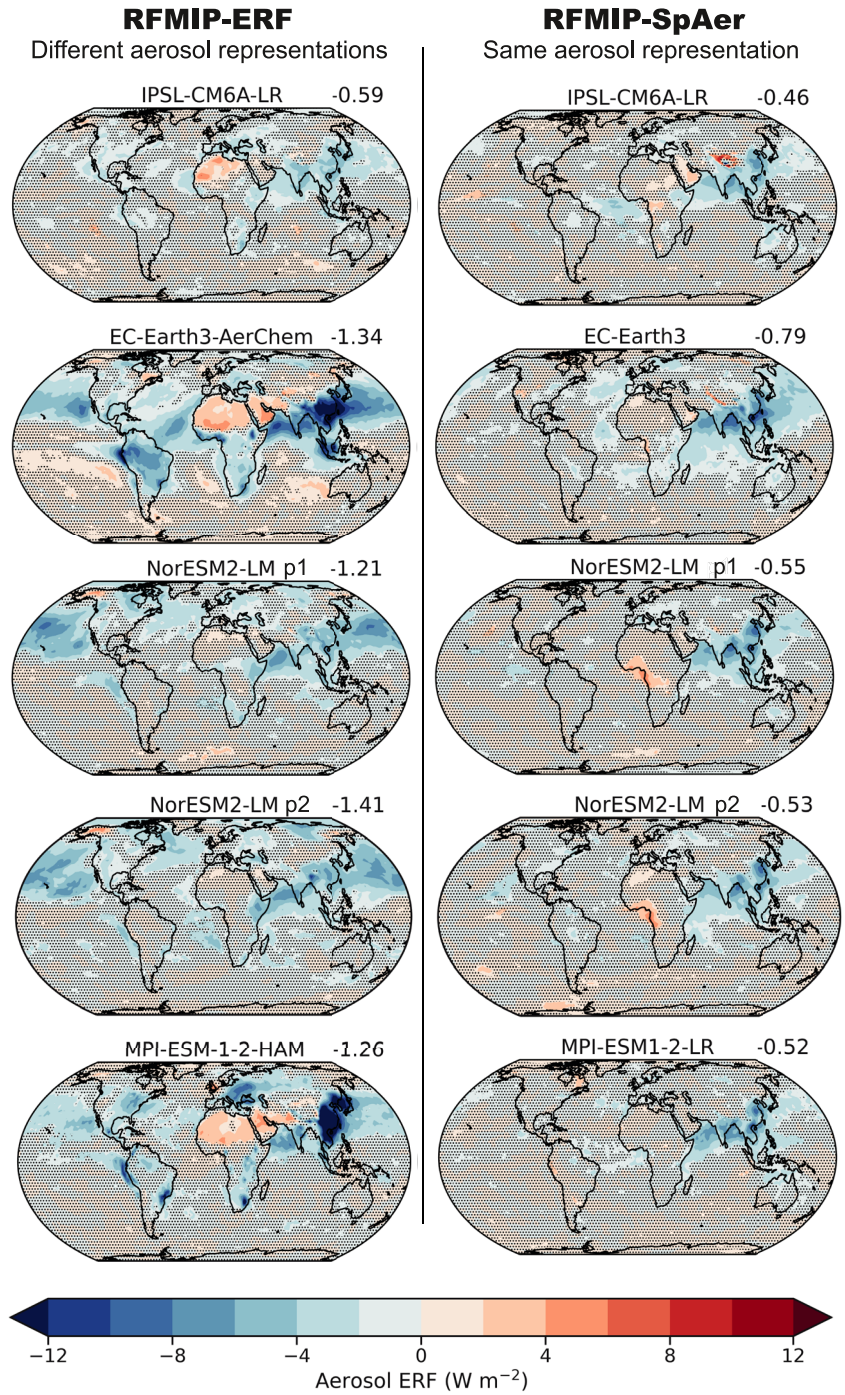

Figure 2. Spatial patterns of the effective radiative effects of present-day anthropogenic aerosols. Shown are (left) a selection of models from RFMIP-ERF against (right) RFMIP-SpAer, based on 30-year-long experiments for the 2014 aerosols (Table S2 in Supporting Information S1). Values in the corner are the global means. Areas without statistically significant values (p-value 0.05) are masked with black dots. All models in RFMIP-ERF are shown in Figure S2 in Supporting Information S1.

Some models in RFMIP-ERF simulate spatial patterns of aerosol $\mathcal{F}$ similar to RFMIP-SpAer. For a systematic assessment of the influence of replacing the anthropogenic aerosol representation of the host model with MACv2-SP, we compare the patterns of aerosol $\mathcal{F}$ between RFMIP-SpAer and the corresponding models in RFMIP-ERF (Figure 2). That comparison gives qualitatively similar results like described for the mean over the entire ensemble, for example, less negative aerosol $\mathcal{F}$ in EC-Earth3 and MPI-ESM1.2 over East Asia compared

to EC-Earth3-AerChem and MPI-ESM1.2-HAM. Moreover, the direct comparison allows us to see more detailed changes. Specifically, the aerosol $\mathcal{F}$ strongly differs in the RFMIP-ERF models but such differences are removed in RFMIP-SpAer, for example, the strongly negative $\mathcal{F}$ in a few model-dependent land regions, for example, South America in EC-Earth3 and North America in MPI-ESM1.2.

3.3. Contributions From Cloud-Mediated Effects

Cloud-mediated effects primarily determine the magnitude of aerosol $\mathcal{F}$ in RFMIP-ERF. For illustration, we decompose aerosol $\mathcal{F}$ into estimates for the direct radiative effects, cloud-mediated effects, and residual effects such as surface albedo adjustments following Ghan (2013) for twelve RFMIP-ERF models with the necessary output. Processes other than direct and cloud-mediated effects to aerosol $\mathcal{F}$ (residual effects) are relatively small (Table S3 in Supporting Information S1) and are not further discussed. The decomposition results underline cloud-mediated effects being substantially larger than the direct effects of aerosols by a factor of two to ten in the global mean (Table S3 in Supporting Information S1). Simulated spatial details vary, but cloud-mediated effects are apparent over ocean regions downwind of major centers of continental pollution in all RFMIP-ERF models, except in the four models of CNRM and GFDL (Figure S5 in Supporting Information S1).

Adjustments due to *aci* can substantially contribute to negative aerosol radiative effects in RFMIP-ERF. This is for instance indicated by the comparisons of experiments of EC-Earth3 and NorESM2 for RFMIP-ERF against their experiments for RFMIP-SpAer (Figure 3). In RFMIP-SpAer, NorESM2-LM accounts for aerosol-radiation interactions and the Twomey effect but does not simulate adjustments due to *aci*. In this case, NorESM2-LM has less negative cloud-mediated effects of -0.19 Wm^{-2} in the global mean than direct effects of -0.34 Wm^{-2}. The effects are substantially different in NorESM2-LM with the native aerosol treatment in RFMIP-ERF, with namely positive direct effects summing to a slightly positive global mean of 0.04 Wm^{-2} paired with negative cloud-mediated effects of -1.38 Wm^{-2} in the global mean. This result hints at strong adjustments due to *aci* with the native aerosol treatment of NorESM2-LM that are eliminated in the corresponding RFMIP-SpAer experiment (Figure 3). Comparing EC-Earth3 results also points to a dominant role of adjustments due to *aci* in the CMIP6 experiment of the model. In the configuration for RFMIP-SpAer, EC-Earth3 accounts for all adjustments induced by MACv2-SP including adjustments via in-cloud processes. In this case, the model has a spatial pattern of negative cloud-mediated effects over oceans that is more similar to many RFMIP-ERF models than to the other RFMIP-SpAer models, which suppress adjustments via in-cloud processes (Figure 3 and Figure S5 in Supporting Information S1). Still, EC-Earth3 has more negative cloud-mediated effects in the experiment for RFMIP-ERF than in RFMIP-SpAer. We typically see larger differences in the magnitude of cloud-mediated effects and direct effects in RFMIP-ERF models, in contrast to RFMIP-SpAer where the global means of the two effects are more similar (Figure 3). Adjustments due to *aci* can therefore substantially contribute to the aerosol ERF in many CMIP6 models (RFMIP-ERF), although this is not true for all, for example, the CNRM models (Figure S5 in Supporting Information S1).

Even when adjustments due to *aci* are not simulated, regionally strong cloud adjustments occur that lead to pronounced negative aerosol $\mathcal{F}$. Specifically, IPSL-CM6A-LR in RFMIP-SpAer has negative aerosol $\mathcal{F}$ over the equatorial Atlantic, which is not seen in the other RFMIP-SpAer models (Figure 2). To some degree, this result was not expected since adjustments due to *aci* are suppressed in the RFMIP-SpAer experiment of IPSL-CM6A-LR, and IPSL-CM6A-LR has overall less pronounced changes in aerosol ERF compared to other models when we go from RFMIP-ERF to RFMIP-SpAer. To gain insights into the reasons for the model behavior over the equatorial Atlantic, we decompose the all-sky $\mathcal{F}$ into a net contribution from cloudy and clear skies and calculate the net contribution from adjustments ($\mathcal{A}$). Over the equatorial Atlantic, we see negative $\mathcal{A}$ right around where the negative cloudy-sky $\mathcal{F}$ occurs in IPSL-CM6A-LR (Figure S3–S4 in Supporting Information S1). Here, adjustments cause an increase in cloud cover (f), which allows the Twomey effect to more strongly contribute to ERF (Figure S4 in Supporting Information S1). Differences in f arise in the RFMIP-SpAer experiment of IPSL-CM6A-LR from adjustments of the atmospheric dynamics to the aerosol-induced heating rates, not via in-cloud microphysical processes. The result for IPSL-CM6A-LR is, therefore, an example of cloud adjustments to aerosol effects on radiation that are opposite in sign compared to cloud burnoff. Similarly in MPI-ESM1.2-LR, we see a moderate increase in cloud cover in the Eastern equatorial Atlantic paired with a co-located regionally pronounced contribution from $\mathcal{A}$ (Figures S3–S4 in Supporting Information S1). Such regional effects like over the equatorial Atlantic could be mistaken for strong adjustments due to *aci* in the form of an extended cloud lifetime if it would occur in a model that simulates all aerosol effects.

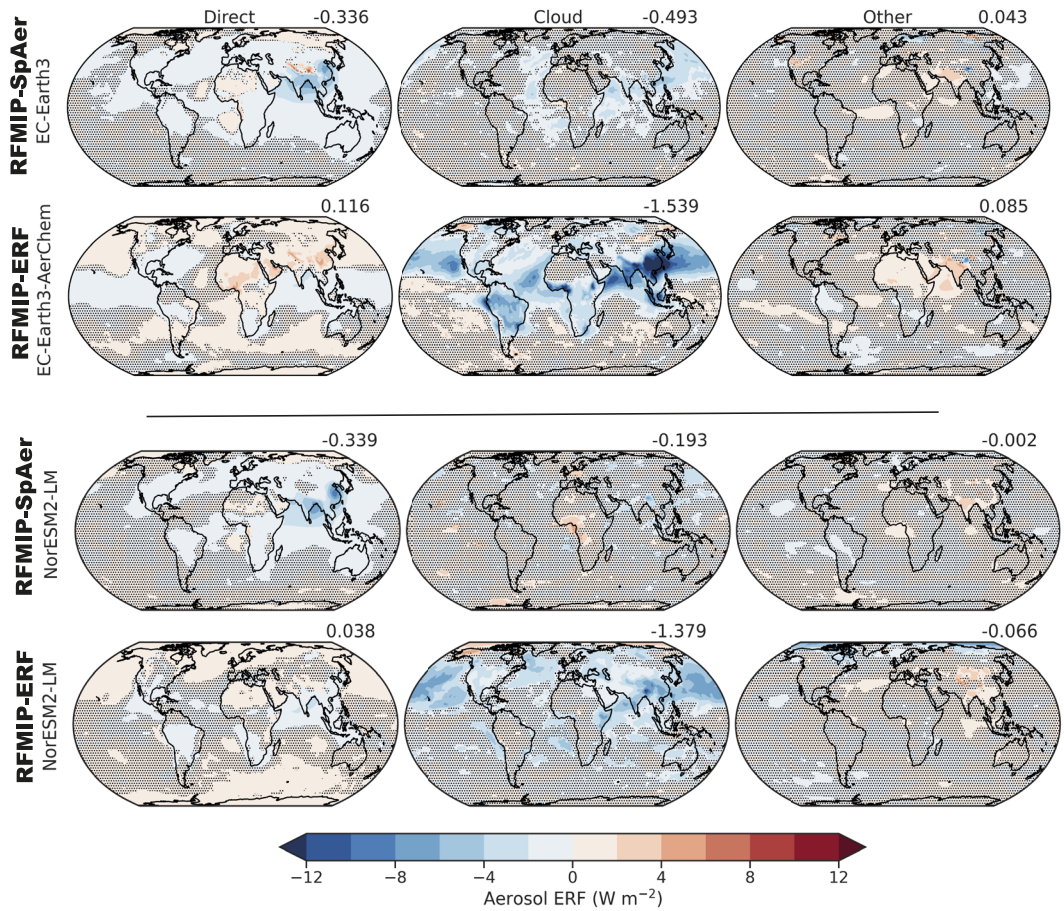

Figure 3. Spatial patterns of present-day anthropogenic aerosol effects. Shown are (left to right) direct, cloud-mediated, and residual effects associated with anthropogenic aerosols at TOA for corresponding model experiments of (top) EC-Earth3 and (bottom) NorESM2-LM p2 in RFMIP-SpAer and RFMIP-ERF, based on 30-year-long experiments for the 2014 aerosols (Table S3 in Supporting Information S1). The decomposition of the effects follows the method by Ghan (2013). Values in the corner are the global means. Areas without statistically significant values (p-value 0.05) are masked with black dots. Contributions for all model experiments in RFMIP-ERF are shown in Figure S5 in Supporting Information S1.

3.4. Contributions From Direct Effects

The direct aerosol effects, although typically smaller in magnitude than cloud-mediated effects, range from negative to positive across RFMIP-ERF, resulting in a multi-model global mean and median close to zero. As discussed in the following, the range in direct forcing stems primarily from different representations of natural and anthropogenic aerosol absorption. In some models, we see a large global mean absorption aerosol optical depth at 550 nm (τ_{abs}) with CanESM5 and GFDL-ESM4 having the largest values of 0.014 and 0.009, while other models have values as low as 0.002 (Table S3 in Supporting Information S1), broadly consistent with τ_{abs} from other assessments (Samset, 2022). The inter-model range in τ_{abs} from RFMIP-ERF translates to differences by a factor of seven. Compared against the τ_{abs} bounds of 0.0025–0.005 from multiple lines of evidence (Bellouin et al., 2020), 9 out of 18 models simulate too strong aerosol absorption. Denoting the global mean aerosol optical depth at 550 nm by τ, the simulated pre-industrial to present-day changes in this quantity ($\Delta\tau$) agree with the range of 0.02–0.04 from Bellouin et al. (2020), except in CESM2 and GISS-E2-1-G. The difference in τ_{abs} is therefore rather associated with the representation of the single scattering albedo of anthropogenic aerosols, denoted as $\omega_0(ant)$, the natural to the anthropogenic fraction in τ_{abs}, or both.

CMIP6 models with positive direct radiative forcing mostly simulate strong anthropogenic aerosol absorption and equal or larger shares of anthropogenic aerosols in τ_{abs} compared to natural aerosols. In CanESM5, EC-Earth3-AerChem, and GFDL-ESM4, anthropogenic aerosols dominate τ_{abs} (Table S3 in Supporting Information S1), that

is, $\frac{\tau_{abs}(nat)}{\tau_{abs}(ant)} < 1$, and these are particularly strongly absorbing with the lowest global mean $\omega_0(ant)$ of 0.77–0.89 across RFMIP-ERF, which are values that have sometimes been observed for biomass burning events (Brown et al., 2021). The strong anthropogenic aerosol absorption is consistent with the positive direct effects, for example, CanESM5 and GFDL-ESM4 have the largest positive direct forcing of 0.26–0.38 Wm^{-2}. For some models including the three mentioned above, we also have output to estimate the global mean mass absorption coefficient (MAC, Table S3 in Supporting Information S1) of anthropogenic black carbon (BC), based on the assumption that the global mean change in the pre-industrial to present-day change in τ_{abs} can be attributed to an increase in BC from anthropogenic sources. Because the required output is not available from all models, we also provide an alternative estimate based on the global τ_{abs} and BC load for the present-day MAC of BC (Table S3 in Supporting Information S1). In GFDL-ESM4, MAC of anthropogenic BC alone is 17 $m^2\ g^{-1}$ that exceeds the maximum of 15 $m^2\ g^{-1}$ for the present-day MAC of total BC simulated in AeroCom (Gliß et al., 2021). Moreover, CanESM5 falls outside of the $\tau_{abs}(ant)$ range and GFDL-ESM4 is at the upper bound from Bellouin et al. (2020). Likewise, EC-Earth3-AerChem falls with 12 $m^2\ g^{-1}$ for MAC of anthropogenic BC alone at the upper end of the range of 3.1–15 $m^2\ g^{-1}$ for MAC of total BC for present-day from AeroCom (Gliß et al., 2021). Again this result is consistent with positive direct effects, for example, over East Asia that are removed when the anthropogenic aerosol optical properties are differently represented in the RFMIP-SpAer experiment of EC-Earth3 (compare Figure 3).

Natural and anthropogenic aerosols about equally contribute to τ_{abs}, that is, $\frac{\tau_{abs}(nat)}{\tau_{abs}(ant)} \approx 1$, in GFDL-CM4, MPI-ESM1-2-HAM, UKESM1-0-LL, NorESM2-MM, and NorESM2-LM p1 and p2. In all these models except UKESM1-0-LL, the direct forcing is positive, although less compared to the models with $\frac{\tau_{abs}(nat)}{\tau_{abs}(ant)} < 1$ which is consistent with the larger $\omega_0(ant)$ of 0.90–0.93 (Table S3 in Supporting Information S1). Still, GFDL-CM4 (19.34 $m^2\ g^{-1}$) and also UKESM1-0-LL (18.56 $m^2\ g^{-1}$) have much larger MAC of anthropogenic BC than seen for the total BC in AeroCom, whereas MPI-ESM1-2-HAM and the NorESM configurations fall with about 8–10 $m^2\ g^{-1}$ for MAC of anthropogenic BC alone onto the upper end of the range of MAC of total BC in AeroCom (Gliß et al., 2021). Specifically, 4 of 9 models with output to compute the present-day MAC of total BC in RFMIP-ERF fall within the range from AeroCom (Gliß et al., 2021), and four models have much larger values of 20–29 $m^2\ g^{-1}$ (CESM2, GFDL-CM4, GFDL-ESM4, UKESM1-0-LL). Anthropogenic BC explains most of the MAC of total BC for present-day in all RFMIP-ERF models with available output, except in MIROC6 (Table S2 in Supporting Information S1). On the contrary, the three models with a dominant role of natural aerosols in τ_{abs} (CNRM-CM6-1, CNRM-ESM2-1, MRI-ESM2-0), that is, $\frac{\tau_{abs}(nat)}{\tau_{abs}(ant)} > 1.5$, have negative direct forcing, consistent with bounds from Bellouin et al. (2020). These results suggest an overestimation of absorption by anthropogenic BC paired with a strong contribution of anthropogenic aerosols in present-day τ_{abs} in many CMIP6 models for which the diagnostic output was available.

4. Discussion and Conclusions

Our results highlight no strong trend in aerosol ERF for 1970–2014 in the CMIP6 multi-model mean, despite strong regional changes in aerosol radiative effects, for example, between the mid-1970s and the mid-2000s (e.g., Fiedler et al., 2019). We see a stabilization of the total anthropogenic ERF in the period 1930–1960 in the CMIP6 multi-model mean. Some models show near zero or negative total anthropogenic ERF around the 1960s and 1970s, consistent with strongly negative present-day aerosol ERF. Trends in ERF reported here from CMIP6 historical experiments might be revised in the future due to updated emission data and model improvements. For instance, regional τ in CMIP6 improved compared to CMIP5 (Cherian & Quaas, 2020), although the improvements in present-day τ are not systematic across different metrics and against several observational data sets (Vogel et al., 2022).

Our results further suggest that the magnitude of cloud-mediated effects primarily explains differences in aerosol ERF across CMIP6, and masks positive direct radiative effects in many CMIP6 models. The intercomparison of model results points for instance to the role of adjustments due to aerosol-cloud interactions over oceans downwind of continental pollution. Differences in direct effects are smaller across CMIP6 when compared to the cloud-mediated effects. Still, direct effects diverge among the models such that direct effects act to warm in eight models and cool only in four models. The positive direct effects arise from excessive contributions of anthropogenic aerosol absorption due to low single scattering albedo for anthropogenic aerosols, for example, from large absorption contributions of anthropogenic black carbon, and low shares of natural aerosol absorption.

Since positive direct aerosol radiative forcing is in disagreement with the assessment by Bellouin et al. (2020), revisiting aerosol optical properties and the share of natural and anthropogenic aerosol absorption can be opportunities to further constrain ERF in CMIP-class models. In so doing, the cloud-mediated effects of aerosols might also change, since clouds adjust to aerosol-induced heating rates from aerosol effects on the radiation transfer. Specifically, our results point to a regional increase in marine cloud cover due to aerosols in an experiment without adjustments due to aerosol-cloud interactions. These adjustments are strong enough to induce marked negative aerosol effective radiative effects away from regions with large τ and with the regional surface-temperature adjustments suppressed. This result is interesting considering that it occurs in a model with an aerosol ERF toward the less negative bound from Bellouin et al. (2020). Future work on aerosol ERF should therefore also address the simulated long-range transport of aerosols over oceans. Precipitation and circulation respond to regional aerosol effects but model results differ, for example, for absorption aerosol optical depth and responses of monsoon precipitation to aerosols in CMIP6 historical experiments (e.g., Monerie et al., 2023; Samset, 2022). Constraining simulated aerosol absorption and transport with the help of observations could therefore facilitate a better understanding of regional climate responses to anthropogenic forcing in future studies.

Data Availability Statement

RFMIP output is freely available via ESGF (https://esgf-data.dkrz.de/search/cmip6-dkrz/). Additional details on the CMIP6 models performing the RFMIP experiments and the analysis methods are in Supporting Information S1.

Acknowledgments
S.F. acknowledges past institutional support from the Max-Planck Institute for Meteorology (MPI-M) and the University of Cologne. T.v.N., D.O., and M.S. acknowledge funding from the European Union's Horizon 2020 research and innovation program under grant agreement No 821205 (FORCeS). C.J.S. was supported by a NERC/IIASA Collaborative Research Fellowship (NE/T009381/1). A.K., D.O., and M.S. were supported by the Research Council of Norway-funded projects INES (270061) and KeyClim (295046). This work used resources of the Deutsches Klimarechenzentrum (DKRZ) granted by its Scientific Steering Committee under project ID bb1198 for data analyses and to MPI-M (mh0730, mh0066) for performing the MPI-ESM1.2-LR experiments. The IPSL-CM6 experiments were performed using the HPC resources of TGCC under the allocations 2019-A0060107732, 2020-A0080107732, and 2021-A0100107732 (project gencmip6) provided by GENCI (Grand Equipement National de Calcul Intensif). T.v.N. analyzed the model output from the *piClim* experiments and C.J.S. from the *hist* experiments. R.P. contributed Figures S1, S3, and S4 in Supporting Information S1. J.-L.D., A.K., A.L., D.O., T.R., A.S., and S.F. performed RFMIP experiments. S.F. led the study and the writing of the manuscript. All authors contributed to the discussion and writing of the manuscript. Open Access funding enabled and organized by Projekt DEAL.

References

Bellouin, N., Quaas, J., Gryspeerdt, E., Kinne, S., Stier, P., Watson-Parris, D., et al. (2020). Bounding global aerosol radiative forcing of climate change. *Reviews of Geophysics*, *58*(1), e2019RG000660. https://doi.org/10.1029/2019RG000660

Bony, S., Stevens, B., Frierson, D. M., Jakob, C., Kageyama, M., Pincus, R., et al. (2015). Clouds, circulation and climate sensitivity. *Nature Geoscience*, *8*(4), 261–268. https://doi.org/10.1038/ngeo2398

Boucher, O., Schwartz, S. E., Ackerman, T. P., Anderson, T. L., Bergstrom, B., Bonnel, B., et al. (1998). Intercomparison of models representing direct shortwave radiative forcing by sulfate aerosols. *Journal of Geophysical Research*, *103*(D14), 16979–16998. https://doi.org/10.1029/98JD00997

Boucher, O., Servonnat, J., Albright, A. L., Aumont, O., Balkanski, Y., Bastrikov, V., et al. (2020). Presentation and evaluation of the IPSL-CM6A-LR climate model. *Journal of Advances in Modeling Earth Systems*, *12*(7), e2019MS002010. https://doi.org/10.1029/2019MS002010

Brown, H., Liu, X., Pokhrel, R., Murphy, S., Lu, Z., Saleh, R., et al. (2021). Biomass burning aerosols in most climate models are too absorbing. *Nature Communications*, *12*(1), 277. https://doi.org/10.1038/s41467-020-20482-9

Cherian, R., & Quaas, J. (2020). Trends in AOD, clouds, and cloud radiative effects in satellite data and CMIP5 and CMIP6 model simulations over aerosol source regions. *Geophysical Research Letters*, *47*(9), e2020GL087132. https://doi.org/10.1029/2020gl087132

Deser, C., Phillips, A. S., Simpson, I. R., Rosenbloom, N., Coleman, D., Lehner, F., et al. (2020). Isolating the evolving contributions of anthropogenic aerosols and greenhouse gases: A new CESM1 large ensemble community resource. *Journal of Climate*, *33*(18), 7835–7858. https://doi.org/10.1175/JCLI-D-20-0123.1

Döscher, R., Acosta, M., Alessandri, A., Anthoni, P., Arsouze, T., Bergman, T., et al. (2022). The EC-Earth3 Earth System Model for the Coupled Model Intercomparison Project 6. *Geoscientific Model Development*, *15*(7), 2973–3020. https://doi.org/10.5194/gmd-15-2973-2022

Eyring, V., Bony, S., Meehl, G. A., Senior, C. A., Stevens, B., Stouffer, R. J., & Taylor, K. E. (2016). Overview of the Coupled Model Intercomparison Project phase 6 (CMIP6) experimental design and organization. *Geoscientific Model Development*, *9*(5), 1937–1958. https://doi.org/10.5194/gmd-9-1937-2016

Fiedler, S., Kinne, S., Huang, W. T. K., Räisänen, P., O'Donnell, D., Bellouin, N., et al. (2019). Anthropogenic aerosol forcing – Insights from multiple estimates from aerosol-climate models with reduced complexity. *Atmospheric Chemistry and Physics*, *19*(10), 6821–6841. https://doi.org/10.5194/acp-19-6821-2019

Fiedler, S., Stevens, B., & Mauritsen, T. (2017). On the sensitivity of anthropogenic aerosol forcing to model-internal variability and parameterizing a Twomey effect. *Journal of Advances in Modeling Earth Systems*, *9*(2), 1325–1341. https://doi.org/10.1002/2017MS000932

Forster, P. M., Richardson, T., Maycock, A. C., Smith, C. J., Samset, B. H., Myhre, G., et al. (2016). Recommendations for diagnosing effective radiative forcing from climate models for CMIP6. *Journal of Geophysical Research*, *121*(20), 12460–12475. https://doi.org/10.1002/2016JD025320

Ghan, S. J. (2013). Technical note: Estimating aerosol effects on cloud radiative forcing. *Atmospheric Chemistry and Physics*, *13*(19), 9971–9974. https://doi.org/10.5194/acp-13-9971-2013

Gliß, J., Mortier, A., Schulz, M., Andrews, E., Balkanski, Y., Bauer, S. E., et al. (2021). AeroCom phase III multi-model evaluation of the aerosol life cycle and optical properties using ground- and space-based remote sensing as well as surface in situ observations. *Atmospheric Chemistry and Physics*, *21*(1), 87–128. https://doi.org/10.5194/acp-21-87-2021

Gulev, S., Thorne, P., Ahn, J., Dentener, F., Domingues, C., Gerland, S., et al. (2021). Changing state of the climate system. In V. Masson-Delmotte, P. Zhai, A. Pirani, S. L. Connors, C. Péan, S. Berger, N. Caud, Y. Chen, L. Goldfarb, M. I. Gomis, M. Huang, K. Leitzell, E. Lonnoy, J. B. R. Matthews, T. K. Maycock, T. Waterfield, O. Yelekçi, R. Yu, & B. Zhou (Eds.), *Climate change 2021: The physical science basis. Contribution of working Group I to the Sixth Assessment Report of the Intergovernmental Panel on Climate Change* (pp. 287–422). Cambridge University Press. https://doi.org/10.1017/9781009157896.004

Kang, S. M., Xie, S.-P., Deser, C., & Xiang, B. (2021). Zonal mean and shift modes of historical climate response to evolving aerosol distribution. *Science Bulletin*, *66*(23), 2405–2411. https://doi.org/10.1016/j.scib.2021.07.013

Liu, L., Shawki, D., Voulgarakis, A., Kasoar, M., Samset, B. H., Myhre, G., et al. (2018). A PDRMIP multimodel study on the impacts of regional aerosol forcings on global and regional precipitation. *Journal of Climate*, *31*(11), 4429–4447. https://doi.org/10.1175/JCLI-D-17-0439.1

Mauritsen, T., Bader, J., Becker, T., Behrens, J., Bittner, M., Brokopf, R., et al. (2019). Developments in the MPI-M Earth System Model version 1.2 (MPI-ESM 1.2) and its response to increasing CO_2. *Journal of Advances in Modeling Earth Systems*, *11*(4), 998–1038. https://doi.org/10.1029/2018MS001400

Monerie, P.-A., Dittus, A. J., Wilcox, L. J., & Turner, A. G. (2023). Uncertainty in simulating twentieth century West African precipitation trends: The role of anthropogenic aerosol emissions. *Earth's Future*, *11*(2), e2022EF002995. https://doi.org/10.1029/2022EF002995

Mülmenstädt, J., Nam, C., Salzmann, M., Kretzschmar, J., L'Ecuyer, T. S., Lohmann, U., et al. (2020). Reducing the aerosol forcing uncertainty using observational constraints on warm rain processes. *Science Advances*, *6*(22), eaaz6433. https://doi.org/10.1126/sciadv.aaz6433

Myhre, G., Samset, B. H., Schulz, M., Balkanski, Y., Bauer, S., Berntsen, T. K., et al. (2013). Radiative forcing of the direct aerosol effect from AeroCom phase II simulations. *Atmospheric Chemistry and Physics*, *13*(4), 1853–1877. https://doi.org/10.5194/acp-13-1853-2013

Neubauer, D., Ferrachat, S., Siegenthaler-Le Drian, C., Stier, P., Partridge, D. G., Tegen, I., et al. (2019). The global aerosol–climate model ECHAM6. 3–HAM2. 3–Part 2: Cloud evaluation, aerosol radiative forcing, and climate sensitivity. *Geoscientific Model Development*, *12*(8), 3609–3639. https://doi.org/10.5194/gmd-12-3609-2019

Pincus, R., Forster, P. M., & Stevens, B. (2016). The radiative forcing model intercomparison project (RFMIP): Experimental protocol for CMIP6. *Geoscientific Model Development*, *9*(9), 3447–3460. https://doi.org/10.5194/gmd-9-3447-2016

Quaas, J., Jia, H., Smith, C., Albright, A. L., Aas, W., Bellouin, N., et al. (2022). Robust evidence for reversal in the aerosol effective climate forcing trend. *Atmospheric Chemistry and Physics*, *22*(18), 12221–12239. https://doi.org/10.5194/acp-22-12221-2022

Randles, C. A., Kinne, S., Myhre, G., Schulz, M., Stier, P., Fischer, J., et al. (2013). Intercomparison of shortwave radiative transfer schemes in global aerosol modeling: Results from the AeroCom radiative transfer experiment. *Atmospheric Chemistry and Physics*, *13*(5), 2347–2379. https://doi.org/10.5194/acp-13-2347-2013

Samset, B. H. (2022). Aerosol absorption has an underappreciated role in historical precipitation change. *Communications Earth & Environment*, *3*(1), 242. https://doi.org/10.1038/s43247-022-00576-6

Samset, B. H., Stjern, C. W., Andrews, E., Kahn, R. A., Myhre, G., Schulz, M., & Schuster, G. L. (2018). Aerosol absorption: Progress towards global and regional constraints. *Current Climate Change Reports*, *4*(2), 65–83. https://doi.org/10.1007/s40641-018-0091-4

Seland, Ø., Bentsen, M., Olivié, D., Toniazzo, T., Gjermundsen, A., Graff, L. S., et al. (2020). Overview of the Norwegian Earth System Model (NorESM2) and key climate response of CMIP6 DECK, historical, and scenario simulations. *Geoscientific Model Development*, *13*(12), 6165–6200. https://doi.org/10.5194/gmd-13-6165-2020

Smith, C. J., Harris, G. R., Palmer, M. D., Bellouin, N., Collins, W., Myhre, G., et al. (2021). Energy budget constraints on the time history of aerosol forcing and climate sensitivity. *Journal of Geophysical Research: Atmospheres*, *126*(13), e2020JD033622. https://doi.org/10.1029/2020JD033622

Smith, C. J., Kramer, R. J., Myhre, G., Alterskjær, K., Collins, W., Sima, A., et al. (2020). Effective radiative forcing and adjustments in CMIP6 models. *Atmospheric Chemistry and Physics*, *20*(16), 9591–9618. https://doi.org/10.5194/acp-20-9591-2020

Stevens, B. (2015). Rethinking the lower bound on aerosol radiative forcing. *Journal of Climate*, *28*(12), 4794–4819. https://doi.org/10.1175/JCLI-D-14-00656.1

Stevens, B., & Feingold, G. (2009). Untangling aerosol effects on clouds and precipitation in a buffered system. *Nature*, *461*(7264), 607–613. https://doi.org/10.1038/nature08281

Stevens, B., Fiedler, S., Kinne, S., Peters, K., Rast, S., Müsse, J., et al. (2017). MACv2-SP: A parameterization of anthropogenic aerosol optical properties and an associated Twomey effect for use in CMIP6. *Geoscientific Model Development*, *10*(1), 433–452. https://doi.org/10.5194/gmd-10-433-2017

Stier, P., Schutgens, N. A. J., Bellouin, N., Bian, H., Boucher, O., Chin, M., et al. (2013). Host model uncertainties in aerosol radiative forcing estimates: Results from the aerocom prescribed intercomparison study. *Atmospheric Chemistry and Physics*, *13*(6), 3245–3270. https://doi.org/10.5194/acp-13-3245-2013

Twomey, S. (1974). Pollution and the planetary albedo. *Atmospheric Environment*, *8*(12), 1251–1256. https://doi.org/10.1016/0004-6981(74)90004-3

Vogel, A., Alessa, G., Scheele, R., Weber, L., Dubovik, O., North, P., & Fiedler, S. (2022). Uncertainty in aerosol optical depth from modern aerosol-climate models, reanalyses, and satellite products. *Journal of Geophysical Research: Atmospheres*, *127*(2), e2021JD035483. https://doi.org/10.1029/2021JD035483

Voigt, A., Albern, N., Ceppi, P., Grise, K., Li, Y., & Medeiros, B. (2021). Clouds, radiation, and atmospheric circulation in the present-day climate and under climate change. *Wiley Interdisciplinary Reviews: Climate Change*, *12*(2), e694. https://doi.org/10.1002/wcc.694

Wang, H., & Wen, Y.-J. (2022). Climate response to the spatial and temporal evolutions of anthropogenic aerosol forcing. *Climate Dynamics*, *59*(5), 1579–1595. https://doi.org/10.1007/s00382-021-06059-2

Wilcox, L. J., Liu, Z., Samset, B. H., Hawkins, E., Lund, M. T., Nordling, K., et al. (2020). Accelerated increases in global and Asian summer monsoon precipitation from future aerosol reductions. *Atmospheric Chemistry and Physics*, *20*(20), 11955–11977. https://doi.org/10.5194/acp-20-11955-2020

Zanis, P., Akritidis, D., Georgoulias, A. K., Allen, R. J., Bauer, S. E., Boucher, O., et al. (2020). Fast responses on pre-industrial climate from present-day aerosols in a CMIP6 multi-model study. *Atmospheric Chemistry and Physics*, *20*(14), 8381–8404. https://doi.org/10.5194/acp-20-8381-2020

Zelinka, M. D., Andrews, T., Forster, P. M., & Taylor, K. E. (2014). Quantifying components of aerosol-cloud-radiation interactions in climate models. *Journal of Geophysical Research: Atmospheres*, *119*(12), 7599–7615. https://doi.org/10.1002/2014JD021710

References From the Supporting Information

Abdul-Razzak, H., & Ghan, S. J. (2000). A parameterization of aerosol activation 2. Multiple aerosol types. *Journal of Geophysical Research*, *105*(D5), 6837–6844. https://doi.org/10.1029/1999JD901161

Bi, D., Dix, M., Marsland, S., O'Farrell, S., Sullivan, A., Bodman, R., et al. (2020). Configuration and spin-up of ACCESS-CM2, the new generation Australian community climate and Earth system simulator coupled model. *Journal of Southern Hemisphere Earth Systems Science*, *70*(1), 225–251. https://doi.org/10.1071/ES19040

Bogenschutz, P. A., Gettelman, A., Hannay, C., Larson, V. E., Neale, R. B., Craig, C., & Chen, C.-C. (2018). The path to CAM6: Coupled simulations with CAM5.4 and CAM5.5. *Geoscientific Model Development*, *11*(1), 235–255. https://doi.org/10.5194/gmd-11-235-2018

Boucher, O., & Lohmann, U. (1995). The sulfate-CCN-cloud albedo effect. *Tellus*, *47B*(3), 281–300. https://doi.org/10.3402/tellusb.v47i3.16048

Boucher, O., Denvil, S., Levavasseur, G., Cozic, A., Caubel, A., Foujols, M.-A., et al. (2022). *IPCC DDC: IPSL IPSL-CM6A-LR-INCA model output prepared for CMIP6 CMIP*. World Data Center for Climate (WDCC) at DKRZ. Retrieved from http://cera-www.dkrz.de/WDCC/ui/Compact.jsp?acronym=C6CMIPILR

Danabasoglu, G., Lamarque, J.-F., Bacmeister, J., Bailey, D. A., DuVivier, A. K., Edwards, J., et al. (2020). The Community Earth System Model version 2 (CESM2). *Journal of Advances in Modeling Earth Systems*, *12*(2), e2019MS001916. https://doi.org/10.1029/2019MS001916

Dunne, J. P., Horowitz, L. W., Adcroft, A. J., Ginoux, P., Held, I. M., John, J. G., et al. (2020). The GFDL Earth System Model version 4.1 (GFDL-ESM 4.1): Overall coupled model description and simulation characteristics. *Journal of Advances in Modeling Earth Systems*, *12*(11), e2019MS002015. https://doi.org/10.1029/2019MS002015

Fiedler, S., Naik, V., O'Connor, F. M., Smith, C. J., Pincus, R., Griffiths, P., et al. (2023). Interactions between atmospheric composition and climate change – Progress in understanding and future opportunities from AerChemMIP, PDRMIP, and RFMIP. In *Geoscientific model development discussions, 2023* (pp. 1–34). https://doi.org/10.5194/gmd-2023-29

Fouquart, Y., & Bonnel, B. (1980). Computations of solar heating of the Earth's atmosphere: A new parametrization. *Contributions to Atmospheric Physics*, *53*, 35–62.

Golaz, J.-C., Caldwell, P. M., Van Roekel, L. P., Petersen, M. R., Tang, Q., Wolfe, J. D., et al. (2019). The DOE E3SM coupled model version 1: Overview and evaluation at standard resolution. *Journal of Advances in Modeling Earth Systems*, *11*(7), 2089–2129. https://doi.org/10.1029/2018MS001603

Halthore, R. N., Crisp, D., Schwartz, S. E., Anderson, G. P., Berk, A., Bonnel, B., & Wiscombe, W. (2005). Intercomparison of shortwave radiative transfer codes and measurements. *Journal of Geophysical Research*, *110*(D11), D11206. https://doi.org/10.1029/2004JD005293

Held, I. M., Guo, H., Adcroft, A., Dunne, J. P., Horowitz, L. W., Krasting, J., et al. (2019). Structure and performance of GFDL's CM4.0 climate model. *Journal of Advances in Modeling Earth Systems*, *11*(11), 3691–3727. https://doi.org/10.1029/2019MS001829

Hourdin, F., Rio, C., Grandpeix, J.-Y., Madeleine, J.-B., Cheruy, F., Rochetin, N., et al. (2020). LMDZ6A: The atmospheric component of the IPSL climate model with improved and better tuned physics. *Journal of Advances in Modeling Earth Systems*, *12*(7), e2019MS001892. https://doi.org/10.1029/2019MS001892

Kelley, M., Schmidt, G. A., Nazarenko, L. S., Bauer, S. E., Ruedy, R., Russell, G. L., et al. (2020). GISS-E2.1: Configurations and climatology. *Journal of Advances in Modeling Earth Systems*, *12*(8), e2019MS002025. https://doi.org/10.1029/2019MS002025

Kinne, S., O'Donnel, D., Stier, P., Kloster, S., Zhang, K., Schmidt, H., et al. (2013). MAC-v1: A new global aerosol climatology for climate studies. *Journal of Advances in Modeling Earth Systems*, *5*(4), 704–740. https://doi.org/10.1002/jame.20035

Kooperman, G. J., Pritchard, M. S., Ghan, S. J., Wang, M., Somerville, R. C. J., & Russell, L. M. (2012). Constraining the influence of natural variability to improve estimates of global aerosol indirect effects in a nudged version of the Community Atmosphere Model 5. *Journal of Geophysical Research*, *117*(D23), D23204. https://doi.org/10.1029/2012JD018588

Mlawer, E. J., Taubman, S. J., Brown, P. D., Iacono, M. J., & Clough, S. A. (1997). Radiative transfer for inhomogeneous atmospheres: RRTM, a validated correlated-k model for the longwave. *Journal of Geophysical Research*, *102*(D14), 16663–16682. https://doi.org/10.1029/97JD00237

Rousset, C., Vancoppenolle, M., Madec, G., Fichefet, T., Flavoni, S., Barthélemy, A., et al. (2015). The Louvain-la-Neuve sea ice model LIM3.6: Global and regional capabilities. *Geoscientific Model Development*, *8*(10), 2991–3005. https://doi.org/10.5194/gmd-8-2991-2015

Séférian, R., Baek, S., Boucher, O., Dufresne, J.-L., Decharme, B., Saint-Martin, D., & Roehrig, R. (2018). An interactive ocean surface albedo scheme: Formulation and evaluation in two atmospheric models. *Geoscientific Model Development*, *11*(1), 321–338. https://doi.org/10.5194/gmd-11-321-2018

Sellar, A. A., Jones, C. G., Mulcahy, J. P., Tang, Y., Yool, A., Wiltshire, A., et al. (2019). UKESM1: Description and evaluation of the U.K. Earth system model. *Journal of Advances in Modeling Earth Systems*, *11*(12), 4513–4558. https://doi.org/10.1029/2019MS001739

Stevens, B., Giorgetta, M., Esch, M., Mauritsen, T., Crueger, T., Rast, S., et al. (2013). Atmospheric component of the MPI-M Earth system model: ECHAM6. *Journal of Advances in Modeling Earth Systems*, *5*(2), 146–172. https://doi.org/10.1002/jame.20015

Swart, N. C., Cole, J. N. S., Kharin, V. V., Lazare, M., Scinocca, J. F., Gillett, N. P., et al. (2019). The Canadian Earth System Model version 5 (CanESM5.0.3). *Geoscientific Model Development*, *12*(11), 4823–4873. https://doi.org/10.5194/gmd-12-4823-2019

Tatebe, H., Ogura, T., Nitta, T., Komuro, Y., Ogochi, K., Takemura, T., et al. (2019). Description and basic evaluation of simulated mean state, internal variability, and climate sensitivity in MIROC6. *Geoscientific Model Development*, *12*(7), 2727–2765. https://doi.org/10.5194/gmd-12-2727-2019

van Noije, T., Bergman, T., Sager, L. P., O'Donnell, D., Makkonen, R., Gonçalves-Ageitos, M., & Yang, S. (2021). EC-Earth3-AerChem: A global climate model with interactive aerosols and atmospheric chemistry participating in CMIP6. *Geoscientific Model Development*, *14*(9), 5637–5668. https://doi.org/10.5194/gmd-14-5637-2021

Voldoire, A., Saint-Martin, D., Sénési, S., Decharme, B., Alias, A., Chevallier, M., et al. (2019). Evaluation of CMIP6 DECK experiments with CNRM-CM6-1. *Journal of Advances in Modeling Earth Systems*, *11*(7), 2177–2213. https://doi.org/10.1029/2019MS001683

Williams, K. D., Copsey, D., Blockley, E. W., Bodas-Salcedo, A., Calvert, D., Comer, R., et al. (2018). The met office global coupled model 3.0 and 3.1 (GC3.0 and GC3.1) configurations. *Journal of Advances in Modeling Earth Systems*, *10*(2), 357–380. https://doi.org/10.1002/2017MS001115

Wu, T., Zhang, F., Zhang, J., Jie, W., Zhang, Y., Wu, F., et al. (2020). Beijing climate center earth system model version 1 (BCC-ESM1): Model description and evaluation of aerosol simulations. *Geoscientific Model Development*, *13*(3), 977–1005. https://doi.org/10.5194/gmd-13-977-2020

Wyser, K., van Noije, T., Yang, S., von Hardenberg, J., O'Donnell, D., & Döscher, R. (2020). On the increased climate sensitivity in the EC-Earth model from CMIP5 to CMIP6. *Geoscientific Model Development*, *13*(8), 3465–3474. https://doi.org/10.5194/gmd-13-3465-2020

Yukimoto, S., Kawai, H., Koshiro, T., Oshima, N., Yoshida, K., Urakawa, S., et al. (2019). The Meteorological Research Institute Earth System Model version 2.0, MRI-ESM2.0: Description and basic evaluation of the physical component. *Journal of the Meteorological Society of Japan. Ser. II*, *97*(5), 931–965. https://doi.org/10.2151/jmsj.2019-051

Ziehn, T., Chamberlain, M. A., Law, R. M., Lenton, A., Bodman, R. W., Dix, M., et al. (2020). The Australian Earth System Model: Access-ESM1.5. *Journal of Southern Hemisphere Earth Systems Science*, *70*(1), 193–214. https://doi.org/10.1071/ES19035